# Diagnostic Accuracy of MR Spectroscopic Imaging and <sup>18</sup>F-FET PET for Identifying Glioma - A Biopsy-Controlled Hybrid PET/MRI Study



University of Cologne, Cologne, Germany

<sup>5</sup> Institute of Neuropathology, Faculty of Medicine and University Hospital Cologne, University

of Cologne, Cologne, Germany

<sup>6</sup> Institute of Neuropathology, University Hospital Düsseldorf and Medical Faculty, Heinrich

Heine University Düsseldorf, Düsseldorf, Germany

<sup>7</sup> Department of Nuclear Medicine, RWTH Aachen University Hospital, Aachen, Germany

<sup>8</sup> Center for Integrated Oncology (CIO), Universities of Aachen, Bonn, Cologne, and

Duesseldorf, Germany

<sup>9</sup> Department of Neurology, Faculty of Medicine and University Hospital Cologne, University

of Cologne, Cologne, Germany

<sup>10</sup> Department of Radiology and Nuclear Medicine, Maastricht University Medical Center

(MUMC+), Maastricht, The Netherlands

<sup>11</sup> Department of Neurology, University Hospital RWTH Aachen, Aachen, Germany

<sup>12</sup> JARA-BRAIN-Translational Medicine, Aachen, Germany

# For correspondence or reprints contact

Jörg Mauler, MD, PhD

Institute of Neuroscience and Medicine (INM-4)

Forschungszentrum Juelich (FZJ)

52425 Juelich, Germany

Email: j.mauler@fz-juelich.de

Phone: +49 2461 612984

Fax: +49 2461 618294

#### **Funding**

No external funding

#### **ABSTRACT**

Contrast-enhanced MRI is the method of choice for brain tumor diagnostics, despite its low specificity for tumor tissue. This study compared the contribution of MR spectroscopic imaging (MRSI) and amino acid PET to improve the detection of tumor tissue. Methods: In 30 untreated patients with suspected glioma, O-(2-[18F]fluoroethyl)-L-tyrosine (18F-FET) PET, 3T-MRSI with short echo time, FLAIR, T2-, and contrast-enhanced T1-weighted MRI were performed for stereotactic biopsy planning. Serial samples were taken along the needle trajectory, and their masks were projected to the preoperative imaging data. Each sample was individually evaluated neuropathologically. <sup>18</sup>F-FET uptake and the MRSI signals choline (Cho), N-acetylaspartate (NAA), creatine, myo-inositol, and derived ratios were evaluated for each sample and classified using logistic regression. The diagnostic accuracy was evaluated by receiver operating characteristic (ROC) analysis. Results: Based on the neuropathological evaluation of tissue from 88 stereotactic biopsies, supplemented with <sup>18</sup>F-FET PET and MRSI metrics from 20 areas on the healthy-appearing contralateral hemisphere to balance the glioma/nonglioma groups, <sup>18</sup>F-FET PET identified glioma with the highest accuracy (area under the ROC curve (AUC) 0.89; confidence interval (CI) 0.81-0.93; threshold, 1.4 x background uptake). Among the MR spectroscopic metabolites, Cho/NAA normalized to normal brain tissue showed the highest diagnostic accuracy (AUC 0.81; CI 0.71-0.88; threshold 2.2). The combination of <sup>18</sup>F-FET PET and normalized Cho/NAA did not improve the diagnostic performance. Conclusions: MRI-based delineation of gliomas should preferably be supplemented by <sup>18</sup>F-FET PET.

#### **KEYWORDS**

MR spectroscopic imaging; <sup>18</sup>F-FET PET; brain tumors; multimodal imaging; stereotactic biopsy

#### **INTRODUCTION**

Currently, contrast-enhanced magnetic resonance imaging (MRI) is the method of choice for the diagnosis and treatment monitoring of patients with brain tumors,(1) but the differentiation between the tumor center, infiltration zone, and peritumoral tissue changes, such as edema, may be challenging, particularly in patients with non-enhancing gliomas.(2) Consequently, the accurate delineation of the glioma extent based on conventional MRI alone may be challenging. Accurate imaging-based tumor localization is essential for treatment planning and for identifying the most metabolically active parts for biopsy planning,(3,4) especially when biopsy sampling is difficult, e.g., in the brain stem(5).

Advanced MRI methods and amino acid PET are of clinical value to obtain additional diagnostic information in clinically challenging situations (*6*). Amino acid PET has been recommended as a supplementary method to structural MRI in brain tumor diagnostics by the Response Assessment in Neuro-Oncology working group.(7) In contrast to [<sup>18</sup>F]-2-fluoro-2-deoxy-D-glucose (<sup>18</sup>F-FDG), the uptake of radiolabeled amino acids is low in normal brain tissue, and brain tumors can be depicted with a high tumor-to-background contrast. Key features of common amino acid tracers such as O-(2-[<sup>18</sup>F]fluoroethyl)-L-tyrosine (<sup>18</sup>F-FET) is their ability to pass through the intact blood-brain barrier, which enables the depiction of the tumor mass beyond contrast enhancement on MRI and of non-enhancing gliomas (*6*,*8*). Local maxima of <sup>18</sup>F-FET uptake in heterogeneous gliomas usually colocalize with the highest <sup>18</sup>F-FDG uptake, but <sup>18</sup>F-FET-PET is considerably more sensitive than <sup>18</sup>F-FDG-PET for biopsy guidance (*6*).

Another approach for detecting neoplastic tissue with high accuracy is the use of metabolic markers derived from MR spectroscopic imaging (MRSI) (9). Most commonly, the MR signal of increased total choline (Cho), which reflects the abnormal choline metabolism in cancers, (10) is used as a marker of malignant transformation. However, the congruency between the tumor borders delineated by the increased Cho to the NAA ratio measured using

MRS compared to <sup>18</sup>F-FET uptake has been investigated in only a few studies. The comparison of 2D spatially resolved MRSI and <sup>18</sup>F-FET uptake showed a congruency greater than 75% in 15 patients with gliomas.(*11*) In contrast to that finding, a study using 3D volumetric brain MRSI found a low level of overlap, 40%, and an average distance of 0.9 cm between the centers of mass of both modalities.(*12*)

Recently, the combination of conventional and advanced MRI methods, as well as <sup>18</sup>F-FET PET, was investigated in a biopsy-controlled study, but the added value of MRSI could not be assessed owing to missing spectroscopic data from the tumor area.(13)

The aim of this study was to investigate the diagnostic accuracy of <sup>18</sup>F-FET PET and MRSI and their combined use to identify neoplastic tissue in patients with newly diagnosed lesions indicative of glioma with histopathology as the gold standard. The imaging findings were validated by tissue obtained from spatially correlated stereotactic biopsies, which were mapped into the preoperative imaging data based on coordinates from the stereotactic surgery.

#### **MATERIALS AND METHODS**

#### **Patients**

The study is based on a series of 35 consecutive patients with structural MRI findings indicating glioma in whom a stereotactic biopsy was planned for clinical reasons such as non-enhancing tumors or unclear differential diagnosis. The patients were scheduled for <sup>18</sup>F-FET PET-guided stereotactic biopsy as part of clinical management and underwent hybrid <sup>18</sup>F-FET PET/MRSI before biopsy. Patients with incomplete sets of multimodal data or low spectral quality data were withdrawn from the study. The study adheres to the standards established in the Declaration of Helsinki and was approved by the ethical committee of the Medical Faculty of the RWTH Aachen University (EK 096/18). All patients gave written informed consent prior to the measurement.

#### **MR** Imaging

All studies were carried out on a Siemens (Erlangen, Germany) 3T TIM Trio MR scanner with a Siemens 8-channel head coil. At the time of the <sup>18</sup>F-FET PET measurement, T1-weighted MRI images were acquired before and after the administration of a gadolinium-based contrast agent (Dotarem™, Guerbet, 95943 Roissy, France) in addition to T2-weighted and FLAIR images. See Supplementary Materials for further details.

A second contrast-enhanced T1-weighted MRI scan was acquired just before the stereotactic surgery, and a cranial computed tomography scan was conducted with the attached stereotactic frame for biopsy planning.

#### MR Spectroscopic Imaging

The high-resolution 3D volumetric MRSI acquisition used a spin-echo excitation with echoplanar readout(14), TE = 17.6 ms, acquisition time of 16 min, integrated lipid and water suppression, and covered the cerebrum. The metabolite signals were scaled with an unsuppressed water reference signal from interleaved measurements. See Supplementary Materials for further details.

### **PET Imaging**

The amino acid <sup>18</sup>F-FET was produced and applied as described previously.(*15*) All patients fasted for at least 12 hours prior to the PET measurement and were injected intravenously with 3 MBq/kg body weight of <sup>18</sup>F-FET. The dynamic <sup>18</sup>F-FET PET acquisition over 50 minutes was carried out using a Siemens BrainPET insert.(*16*) See Supplementary Materials for further details. All reconstructed frames (resolution iso 1.25 mm) were smoothed with a 2.5 mm Gaussian kernel, and motion was corrected using PMOD (v3.5, Zürich, Switzerland). The summed images from 20 to 40 minutes post-injection were used for the analysis.

#### **Stereotactic Biopsies**

Before stereotactic biopsy, contrast-enhanced MRI and <sup>18</sup>F-FET PET were spatially registered on an intraoperatively obtained cranial CT as a basic image for planning the biopsy trajectory. The trajectory targeted the area with the highest <sup>18</sup>F-FET uptake while avoiding vessels and eloquent brain areas. The samples were (re)classified according to the 2021 World Health Organization (WHO) Classification of Tumors of the Central Nervous System (CNS) taxonomy.(17) (see Supplementary Materials). The biopsies were taken an average of 11 days after the PET measurements (standard deviation (SD) 11 d, minimal 3 d, maximum 56 d). For ethical reasons, samples could not be taken from healthy brain tissue; thus, the number of control samples was underrepresented. In order to balance the groups of samples for statistical analysis, "virtual negative biopsies" (i.e., the non-invasive examination of healthy-appearing contralateral brain regions using <sup>18</sup>F-FET PET and MRSI) were placed on the contralateral side. See Supplementary Materials for further details.

#### **Data Analysis**

The reconstruction of the spectroscopic data was carried out using the Metabolite Imaging and Data Analysis System (MIDAS) software package.(18) After the interpolation of the raw data to 64 × 64 × 32 voxels (4.375 x 4.375 x 5.625 mm³), the final spatial resolution of 108 mm³ was gained. The data were transformed into volumetric metabolite maps by using automatic spectral analysis and following signal normalization to the simultaneously acquired water reference signal.(19) The maps comprised the metabolite distributions of Cho, Cr, NAA, and myo-Inositol (mIno). For the final analysis, ratio maps of Cho/NAA, NAA/Cr, Cho/Cre, and mIno/Cr were calculated.

The <sup>18</sup>F-FET PET, MRSI, all other MRI data, and the biopsy track masks were registered to the T1 data. Masks of the tumor and the surrounding edema were manually delineated based

on the FLAIR and T2 data (12) and used to keep the normalization to the water signal devoid of distortions caused by the edema of the tumor tissue.

The <sup>18</sup>F-FET uptake and MRSI metabolite data were normalized to the respective background signals, which were given by the mean signal outside of the area delineated by the previously described tumor masks. This procedure is referred to below as normalization to normal-appearing tissue. The normalized <sup>18</sup>F-FET images, <sup>18</sup>F-FET<sub>n</sub>, were resampled to the resolution of the metabolite maps. In addition to the normalized metabolite values, the non-normalized values were analyzed to enable comparison with literature values.

The biopsy masks were down-sampled to match the spatial resolution of the spectroscopic data. Voxels with a biopsy partial volume of less than 50% or an underlying spectral linewidth outside the interval from 3 to 12 Hz were excluded from further analysis.

The histological findings "glial tumor" and "infiltration zone" were labeled as tumor tissue in terms of PET/MRS imaging. Benign results and findings that were positive only on the microscopic scale, such as "proliferated brain tissue with tumor cells", were considered negative.

The threshold for neoplastic tissue based on different metabolite combinations and/or <sup>18</sup>F-FET uptake was determined by logistic regression as described in the Supplementary Material.

#### **RESULTS**

From July 2018 to September 2020, a series of 35 patients with suspected brain tumors were recruited for the study. After the exclusion of four patients because of low spectral quality and one patient because of missing biopsy coordinates, the analyzed group included 30 patients (f/m=14/16) with an average age of  $48 \pm 13$  years (mean  $\pm$  SD; range 27 - 82 years).

Supplementary Table S1 shows the individual characteristics and neuropathological diagnoses according to the 2021 WHO CNS classification (Table S2: patients excluded due to insufficient spectral quality). In total, nine patients with enhancing gliomas, 15 patients with non-enhancing gliomas, two patients with enhancing lesions other than gliomas, and four patients with non-glioma lesions without contrast enhancement were included.

Patient 4 had the contradicting findings of "vasculitis", contrast enhancement, and high <sup>18</sup>F-FET uptake (2.6). As the follow-up biopsy 18 months later showed a glioblastoma (IDH-wildtype (CNS WHO grade 4)), the first biopsy was considered a sampling error, and the later diagnosis was used.

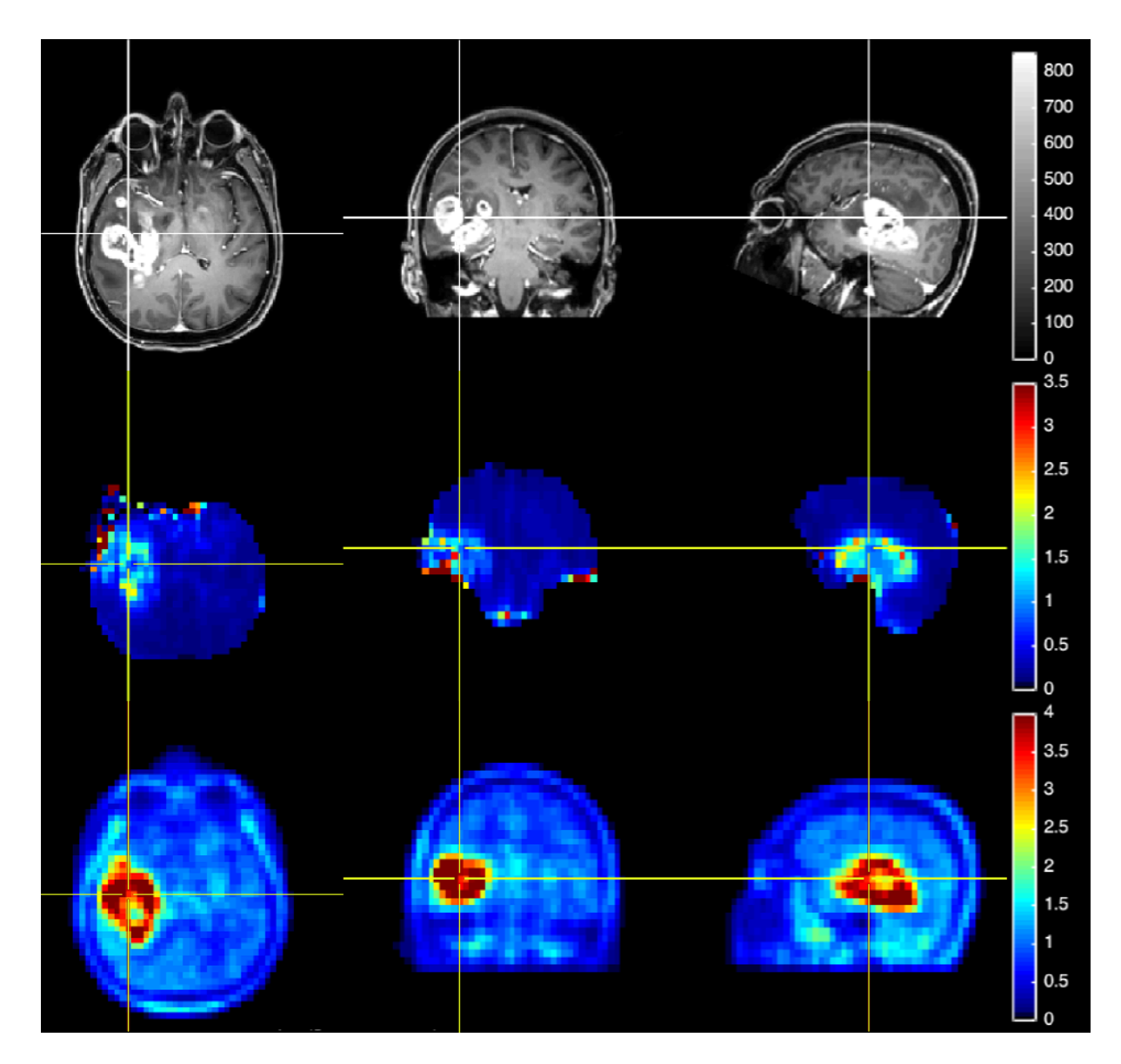


**FIGURE 1.** Example of registered contrast-enhanced T1-weighted MRI (top; arbitrary units), the corresponding Cho/NAA spectroscopic image (middle), and <sup>18</sup>F-FET PET (bottom) of a patient (#18) who was diagnosed with a glioblastoma, IDH-wildtype, CNS WHO grade 4. The <sup>18</sup>F-FET<sub>n</sub> data were resliced and resampled to the resolution of the MRSI data. The position of the crosshair marks the location of the biopsy.

Per patient,  $2.9 \pm 1.2$  (2-7) cylindrical specimens with a diameter of 2.8 mm and a length of 5-10 mm were obtained along 1-2 biopsy trajectories. Eighteen biopsies were excluded because of the low spectral quality of the corresponding MR spectrum. The <sup>18</sup>F-FET PET and MRSI data were acquired 13  $\pm$  12 days before taking the biopsies, and the T1 series for biopsy

planning was measured 3  $\pm$  5 days before surgery. In total, 108 multimodal data sets, comprising 88 real biopsies supplemented with 20 virtual negative biopsies, were included in the analysis. Fifty-four biopsies were neuropathologically evaluated as glioma tissue. Figure 1 shows an example of a multimodal MRSI and  $^{18}$ F-FET data set at spectroscopic imaging resolution and registered to the anatomical T1 data. Since the planning of the biopsy trajectories was based on the  $^{18}$ F-FET uptake and the MRI results, but did not take into account the MRSI results, the biopsy sites did not necessarily coincide with the sites of maximum spectroscopic signals (Figure 2).

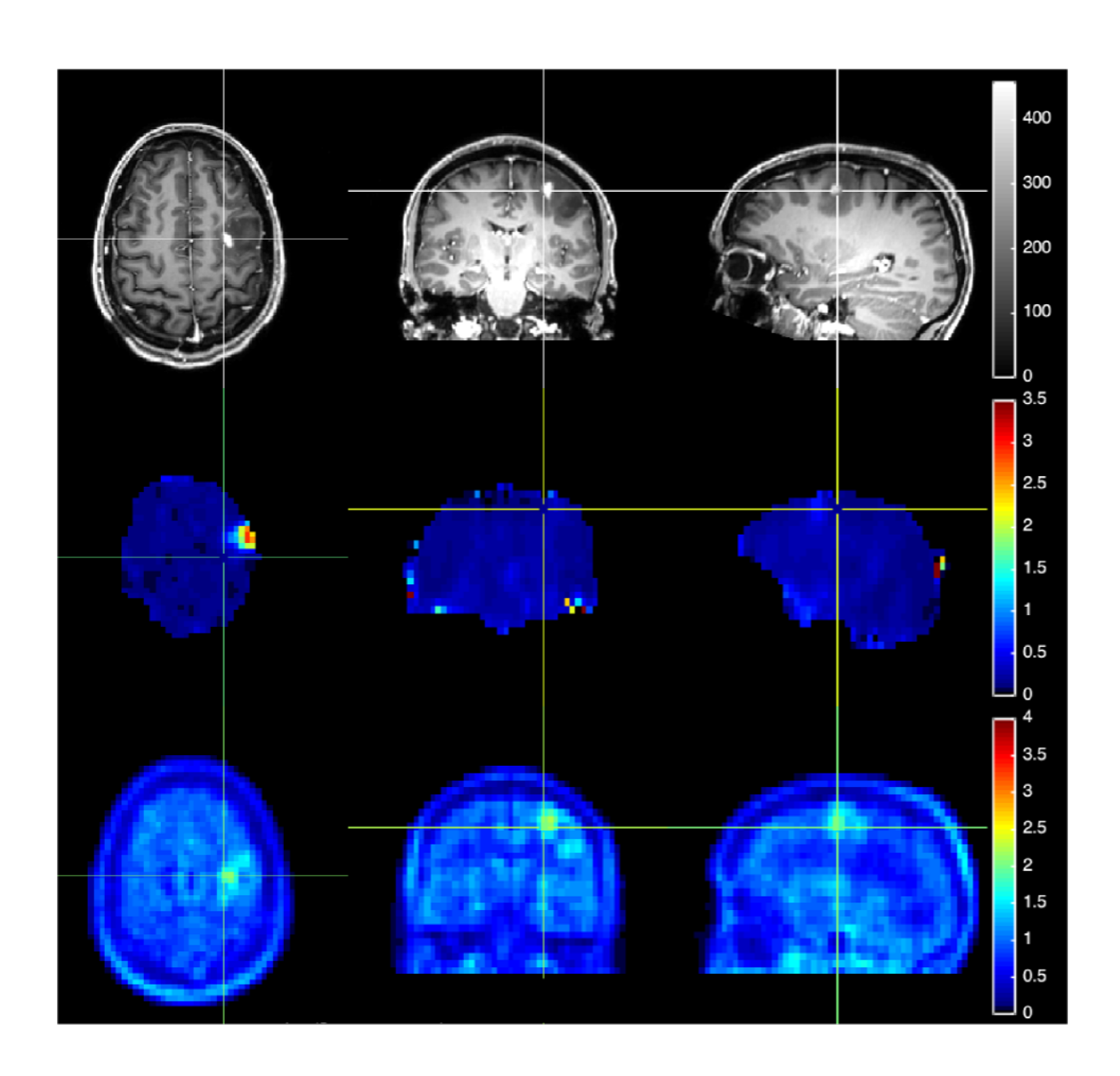


**FIGURE 2.** Contrast-enhanced T1-weighted MRI (top; arbitrary units), registered Cho/NAA spectroscopic signals (middle), and <sup>18</sup>F-FET PET (bottom) from patient 1 diagnosed with an astrocytoma, IDH1-mutant, CNS WHO grade 3. Biopsy positions were planned based on <sup>18</sup>F-FET enhancement and therefore did not necessarily coincide with the sites of maximum Cho/NAA ratios. The position of the crosshair marks the location of the biopsy.

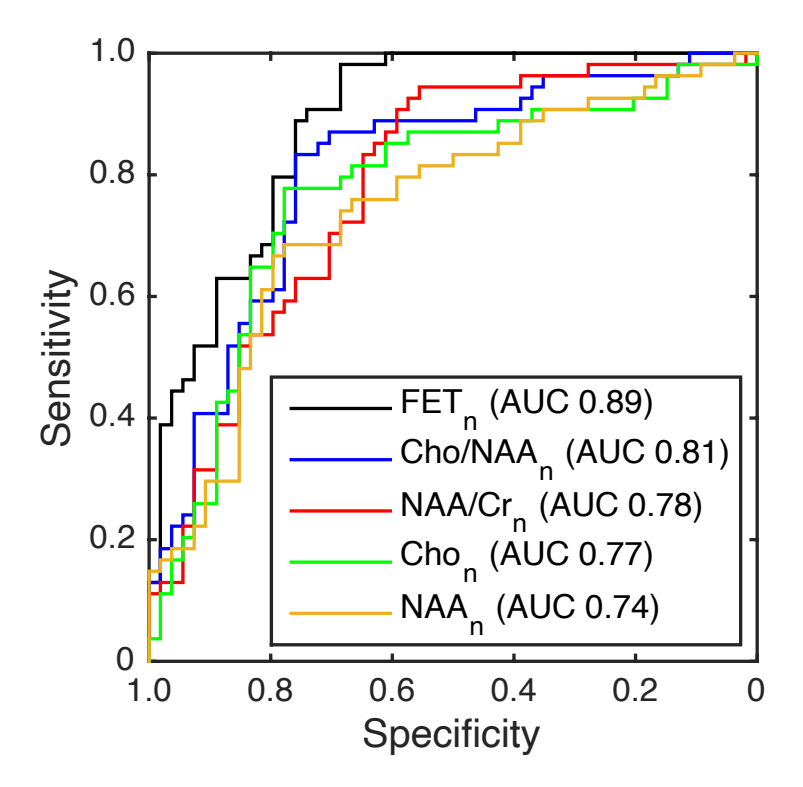


**FIGURE 3.** Receiver operating characteristic curves of <sup>18</sup>F-FET<sub>n</sub> PET and the MRSI metabolic markers Cho/NAA<sub>n</sub>, NAA/Cr<sub>n</sub>, Cho<sub>n</sub>, and NAA<sub>n</sub> based on the analysis of 88 biopsies and 20 imaging data points from normal-appearing brain tissue.

Among the analyses of the single modality data, the uptake of  $^{18}\text{F-FET}_n$  resulted in the highest diagnostic accuracy with an averaged AUC of 0.89 after cross-validation (SD 0.003; confidence interval (CI) 0.81 - 0.93), which is linked to an uptake threshold of 1.4 x background uptake (Tables 1 and 2).

Generally, the accuracy of the metabolite results generated from MRSI increased by up to 0.06 if the signals were normalized to normal-appearing tissue and additionally to another metabolite signal (such as Cho/NAA). When the diagnostic distinction between glial tumor and normal tissue was based on the spectroscopic marker Cho/NAA<sub>n</sub>, the accuracy decreased to an average AUC of 0.81 (SD 0.004; CI 0.71 - 0.88), based on a Cho/NAA<sub>n</sub> threshold of 2.2. All other analyzed spectroscopic signals, NAA/Cr<sub>n</sub> (AUC 0.78), Cho<sub>n</sub> (AUC 0.77), NAA<sub>n</sub> (AUC 0.74), Cho/Cr<sub>n</sub> (AUC 0.72), mIno<sub>n</sub> (AUC 0.70), and mIno/Cr<sub>n</sub> (AUC 0.70), showed lower accuracies. The result of Cr did not pass the significance threshold. The ROC curves of the five highest accuracy values are compared in Figure 3.

The combined analysis of the markers with the highest accuracy,  $^{18}\text{F-FET}_n$  uptake and Cho/NAA<sub>n</sub>, did not pass the significance threshold of p  $\leq$  0.05. The results may indicate the tendency towards slightly improved accuracy (AUC 0.90; Cho/NAA term, p = 0.3) compared to the  $^{18}\text{F-FET}_n$  uptake (AUC 0.89) and Cho/NAA<sub>n</sub> (AUC 0.81) alone. The results obtained after introducing an interaction term between  $^{18}\text{F-FET}_n$  and Cho/NAA<sub>n</sub> are shown in the Supplementary Table S3.

The subgroup analysis of gliomas without contrast enhancement showed a slightly decreased AUC of 0.88 (CI 0.75 - 0.94) when the diagnosis was based on <sup>18</sup>F-FET<sub>n</sub> uptake and an increased AUC of 0.85 (CI 0.72 - 0.93) for Cho/NAA<sub>n</sub>. Compared to the values from all patients, the threshold values dropped to 1.3 for <sup>18</sup>F-FET<sub>n</sub> and increased to 2.3 for Cho/NAA<sub>n</sub>.

Accordingly, compared to the evaluation of the entire group of patients, the restriction to gliomas with contrast enhancement showed a higher diagnostic accuracy of <sup>18</sup>F-FET<sub>n</sub> and a lower accuracy of Cho/NAA<sub>n</sub>. <sup>18</sup>F-FET<sub>n</sub>-based diagnosis resulted in an AUC of 0.91 (CI 0.80 - 0.96; threshold 1.5). Using Cho/NAA<sub>n</sub> for diagnosis resulted in an AUC of 0.77 (CI 0.61 - 0.88; threshold 2.0).

The <sup>18</sup>F-FET<sub>n</sub>-based diagnostics showed more accurate results, with 78% correctly classified samples compared to 71% correct classifications in the leave-one-out cross-validation for Cho/NAA<sub>n</sub> (Table 2). <sup>18</sup>F-FET had superior sensitivity, 76%, whereas Cho/NAA showed better specificity, 83%. The positive predictive value of <sup>18</sup>F-FET<sub>n</sub> uptake was similar (79% versus 78%), and its negative predictive value was higher than that of Cho/NAA<sub>n</sub> (77% versus 67%).

#### **DISCUSSION**

The major finding of this study is the higher diagnostic accuracy of  $^{18}\text{F-FET}_n$  uptake compared to Cho/NAA<sub>n</sub> for the imaging-based diagnosis of tumor tissue in enhancing and non-enhancing gliomas. Optimal glioma delineation was achieved with the  $^{18}\text{F-FET}_n$ -based tumor-to-background ratio of 1.4 and Cho/NAA<sub>n</sub>  $\geq$  2.2.

When <sup>18</sup>F-FET uptake was considered, the trend to the highest diagnostic accuracy was found in enhancing gliomas. Cho/NAA<sub>n</sub> showed a trend to higher accuracy in non-enhancing gliomas but still has a lower value than <sup>18</sup>F-FET<sub>n</sub>. Given the relatively low number of patients, the corresponding overlapping 95%-confidence intervals do not allow a clear statement and may be responsible for the observed counterintuitive tendency of lower accuracy of Cho/NAA<sub>n</sub> in enhancing gliomas. However, the trend towards the higher diagnostic accuracy of <sup>18</sup>F-FET<sub>n</sub> is consistent with previously reported results.(*13*)

Regardless of contrast enhancement, <sup>18</sup>F-FET PET-based diagnosis generally showed higher diagnostic accuracy than Cho/NAA. Hence, <sup>18</sup>F-FET PET is significantly more sensitive for identifying glioma tissue; all be it at the cost of a somewhat lower specificity compared to Cho/NAA.

The selection of metabolites and derived ratios includes those that can be determined with high accuracy at 3T.(20) The individual signals from Cho and NAA showed lower accuracy than their ratio. This is consistent with the finding that while Cho is variably elevated in different glioma types, NAA is reduced non-uniformly as a broad marker of neuronal loss.(21) Compared to Cho/NAA, the other investigated metabolite signals, Cho, NAA, NAA/Cr, Cho/Cr, mlno, and mlno/Cr, generally showed lower accuracy in diagnosing glioma. Frequently, study results are reported as metabolite ratios, such as Cho/NAA, without further normalization. This study showed higher accuracies if signal ratios were additionally normalized to normal-appearing tissue.

Four out of 35 patients (11%) were excluded from the analysis because of insufficient spectral quality. In addition, 18 samples had to be excluded from the remaining group of 106 samples (17%) for the same reason, which reduces the clinical utility of MRSI.

Within the limitations given by a different patient group, the observed <sup>18</sup>F-FET tumor threshold of 1.4 x background uptake confirms the previously reported value and the widely used threshold of 1.6.(22,23) Besides the fact that the threshold values were determined with different PET scanners and influenced by different point spread functions, the current study included fewer subjects and more patients with gliomas showing equivocal findings on MRI. Therefore, the slightly decreased threshold in our study should be considered with caution and requires further biopsy-controlled studies in larger patient groups.

Relatively few studies have calibrated glioma-normal-tissue thresholds using coordinate-controlled biopsies. The found threshold of 0.65 for the absolute Cho/NAA ratio corresponds to the previously published integral ratio (non-proton number corrected) Cho/NAA ≥ 2, which, however, was determined for a longer echo time (135 ms instead of 17 ms) by using spatial 2D MRSI and approximately the threefold measured voxel size from a smaller group of patients.(24) Data acquired with an even larger voxel size and long echo time resulted in the

minimum ratio of 1.3.(25) This value was obtained from predominantly high-grade gliomas and fits as a lower limit to our threshold value.

The accuracy of the results depends on the decision as to which neuropathological findings are considered positive for tumor tissue. In the presented analysis, the presence of single tumor cells in the tissue samples was not rated as tumor tissue because such findings are not accessible with either imaging method due to the limited spatial resolution.

A limitation of this study is the small number of patients included and the large proportion of equivocal MR findings, often due to lacking contrast enhancement. Nevertheless, as these patients are particularly difficult to diagnose, the importance and value of amino acid PET for this group of patients is further emphasized. A further limitation is the study design, which favors <sup>18</sup>F-FET over MRSI, as biopsy tracks were planned based on <sup>18</sup>F-FET PET to target the most metabolically active part of the tumor because MRSI data were not yet available at the time of biopsy. Therefore, the use of MRS data for biopsy planning(26,27) could not be properly compared to that from <sup>18</sup>F-FET PET. A further consequence of the study design was a lack of Cho/NAA positive but <sup>18</sup>F-FET negative samples. Therefore, the relevance of high Cho/NAA with low <sup>18</sup>F-FET uptake, which may indicate gliosis, inflammation and/or demyelination (3,28,29) or the indication of a later recurrence and of reduced progression-free survival,(26,30) remains to be addressed in future studies. Generally, in this study, histology was considered the gold standard defining diagnosis since the biopsies were analyzed by two experienced neuropathologists according to the 2021 WHO Classification of Tumors of the Central Nervous System.

The multimodal approach using MRSI, <sup>18</sup>F-FET PET, and neuropathology necessitates the combination of data from the mm scale down to the sub-mm scale. Only the <sup>18</sup>F-FET PET data can be down-sampled to spectroscopic imaging resolution, whereas the neuropathological results are bound to the dimensions of the biopsy cylinders. Accordingly, possible location

errors are in this order of magnitude. Since the <sup>18</sup>F-FET concentration in the blood compartment is high in the first hour after administration, special attention was paid during the evaluation to ensure that the <sup>18</sup>F-FET signal was not partially confused with an increased signal contribution from blood vessels.(*15*) In rare cases, however, after the resampling of the <sup>18</sup>F-FET data to the resolution of the metabolite maps, the contamination of the larger voxels cannot be completely ruled out. Moreover, the MRSI data bear the MRS inherent chemical shift displacement error. With the given readout gradient of 13.72 mT/m, this error is a fraction of the nominal voxel size in anterior-posterior direction and, therefore, negligible for the analysis in spectroscopic imaging resolution.

#### **CONCLUSION**

Amino acid PET using the tracer <sup>18</sup>F-FET allows the diagnosis and identification of viable glioma tissue with a high diagnostic accuracy. The most accurate tumor delineation for a mixed group of enhancing and non-enhancing gliomas was accomplished with a threshold of <sup>18</sup>F-FET uptake of 1.4 x background signal. MRSI provides the highest diagnostic accuracy with a Cho/NAA<sub>n</sub> threshold of 2.2. Further data are required to assess the possible diagnostic benefit of the combined analysis of <sup>18</sup>F-FET uptake and MRS metabolites, such as Cho/NAA, and to assess the diagnostic meaning of Cho/NAA positive but <sup>18</sup>F-FET negative findings.

#### **DISCLOSURE**

N.G. and P.L. received honoraria for lectures from Blue Earth Diagnostics. N.G. received honoraria for advisory board participation from Telix Pharmaceuticals. K.-J.L and F.M.M. received honoraria for consultancy service from Telix Pharmaceuticals. No other potential conflict of interest.

#### **ACKNOWLEDGEMENTS**

The authors thank Silke Frensch, Kornelia Frey, Natalie Judov, Trude Plum, Suzanne Schaden, and Lutz Tellmann for assistance in the patient studies, and Johannes Ermert, Silke

Grafmüller, Erika Wabbals, and Sascha Rehbein for the radiosynthesis of <sup>18</sup>F-FET. The authors greatly appreciate Claire Rick's English proofreading.

#### **KEY POINTS**

**QUESTION:** What is the diagnostic accuracy of <sup>18</sup>F-FET-PET and MRSI for the detection of glioma?

**PERTINENT FINDINGS:** Validated using tissue samples from stereotactic biopsies, <sup>18</sup>F-FET-PET identified glioma with an accuracy of 0.89. The MRSI marker Cho/NAA showed a diagnostic accuracy of 0.81.

**IMPLICATIONS FOR PATIENT CARE:** MRI-based delineation of gliomas should preferably be supplemented by <sup>18</sup>F-FET PET.

#### **REFERENCES**

- **1.** Pope WB, Brandal G. Conventional and advanced magnetic resonance imaging in patients with high-grade glioma. *Q J Nucl Med Mol Imaging*. 2018;62:239-253.
- **2.** Hygino da Cruz LC, Jr., Rodriguez I, Domingues RC, Gasparetto EL, Sorensen AG. Pseudoprogression and pseudoresponse: imaging challenges in the assessment of posttreatment glioma. *AJNR Am J Neuroradiol.* 2011;32:1978-1985.
- **3.** Floeth FW, Pauleit D, Wittsack H-J, et al. Multimodal metabolic imaging of cerebral gliomas: positron emission tomography with [18F]fluoroethyl-L-tyrosine and magnetic resonance spectroscopy. *J Neurosurg.* 2005;102:318-327.
- **4.** Misch M, Guggemos A, Driever PH, et al. (18)F-FET-PET guided surgical biopsy and resection in children and adolescence with brain tumors. *Childs Nerv Syst.* 2015;31:261-267.
- **5.** Purohit B, Kamli AA, Kollias SS. Imaging of adult brainstem gliomas. *Eur J Radiol.* 2015;84:709-720.
- **6.** Langen KJ, Galldiks N, Hattingen E, Shah NJ. Advances in neuro-oncology imaging. *Nat Rev Neurol.* 2017;13:279-289.
- **7.** Albert NL, Weller M, Suchorska B, et al. Response Assessment in Neuro-Oncology working group and European Association for Neuro-Oncology recommendations for the clinical use of PET imaging in gliomas. *Neuro Oncol.* 2016;18:1199-1208.

- **8.** Lohmann P, Stavrinou P, Lipke K, et al. FET PET reveals considerable spatial differences in tumour burden compared to conventional MRI in newly diagnosed glioblastoma. *Eur J Nucl Med Mol Imaging.* 2019;46:591-602.
- **9.** Widhalm G, Krssak M, Minchev G, et al. Value of H-1-magnetic resonance spectroscopy chemical shift imaging for detection of anaplastic foci in diffusely infiltrating gliomas with non-significant contrast-enhancement. *Journal of Neurology Neurosurgery and Psychiatry*. 2011;82:512-520.
- **10.** Glunde K, Penet M-F, Jiang L, Jacobs MA, Bhujwalla ZM. Choline metabolism-based molecular diagnosis of cancer: an update. *Expert Rev Mol Diagn.* 2015;15:735-747.
- **11.** Stadlbauer A, Nimsky C, Buslei R, et al. Proton magnetic resonance spectroscopic imaging in the border zone of gliomas: correlation of metabolic and histological changes at low tumor infiltration--initial results. *Invest Radiol.* 2007;42:218-223.
- **12.** Mauler J, Maudsley AA, Langen K-J, et al. Spatial Relationship of Glioma Volume Derived from <sup>18</sup>F-FET PET and Volumetric MR Spectroscopy Imaging: A Hybrid PET/MRI Study. *J Nucl Med.* 2018;59:603-609.
- **13.** Verburg N, Koopman T, Yaqub MM, et al. Improved detection of diffuse glioma infiltration with imaging combinations: a diagnostic accuracy study. *Neuro Oncol.* 2020;22:412-422.
- **14.** Ebel A, Maudsley AA. Detection and correction of frequency instabilities for volumetric 1H echo-planar spectroscopic imaging. *Magn Reson Med.* 2005;53:465-469.

- **15.** Langen KJ, Stoffels G, Filss C, et al. Imaging of amino acid transport in brain tumours: Positron emission tomography with O-(2-[18F]fluoroethyl)-L-tyrosine (FET). *Methods*. 2017;130:124-134.
- **16.** Herzog H, Langen K-J, Weirich C, et al. High resolution BrainPET combined with simultaneous MRI. *Nuklearmedizin*. 2011;50:74-82.
- **17.** Louis DN, Perry A, Wesseling P, et al. The 2021 WHO Classification of Tumors of the Central Nervous System: a summary. *Neuro Oncol.* 2021;23:1231-1251.
- **18.** Maudsley AA, Darkazanli A, Alger JR, et al. Comprehensive processing, display and analysis for in vivo MR spectroscopic imaging. *NMR Biomed*. 2006;19:492-503.
- **19.** Soher BJ, Young K, Govindaraju V, Maudsley AA. Automated spectral analysis III: application to in vivo proton MR spectroscopy and spectroscopic imaging. *Magn Reson Med.* 1998;40:822-831.
- **20.** Henning A. Proton and multinuclear magnetic resonance spectroscopy in the human brain at ultra-high field strength: A review. *Neuroimage*. 2017.
- **21.** Dowling C, Bollen AW, Noworolski SM, et al. Preoperative proton MR spectroscopic imaging of brain tumors: correlation with histopathologic analysis of resection specimens. *AJNR Am J Neuroradiol*. 2001;22:604-612.
- **22.** Rapp M, Heinzel A, Galldiks N, et al. Diagnostic performance of 18F-FET PET in newly diagnosed cerebral lesions suggestive of glioma. *J Nucl Med.* 2013;54:229-235.

- **23.** Pauleit D, Floeth F, Hamacher K, et al. O-(2-[18F]fluoroethyl)-L-tyrosine PET combined with MRI improves the diagnostic assessment of cerebral gliomas. *Brain.* 2005;128:678-687.
- **24.** Guo J, Yao C, Chen H, et al. The relationship between Cho/NAA and glioma metabolism: implementation for margin delineation of cerebral gliomas. *Acta Neurochir (Wien)*. 2012;154:1361-1370.
- **25.** Vigneron D, Bollen A, McDermott M, et al. Three-dimensional magnetic resonance spectroscopic imaging of histologically confirmed brain tumors. *Magn Reson Imaging*. 2001;19:89-101.
- **26.** Zhong J, Huang V, Gurbani SS, et al. 3D whole-brain metabolite imaging to improve characterization of low-to-intermediate grade gliomas. *J Neurooncol.* 2021;153:303-311.
- **27.** Abdelaziz O, Eshra M, Belal A, Elshafei M. Diagnostic Value of Magnetic Resonance Spectroscopy Compared with Stereotactic Biopsy of Intra-axial Brain Lesions. *J Neurol Surg A Cent Eur Neurosurg.* 2016;77:283-290.
- **28.** Hayashi T, Kumabe T, Jokura H, et al. Inflammatory demyelinating disease mimicking malignant glioma. *J Nucl Med.* 2003;44:565-569.
- **29.** Majós C, Aguilera C, Alonso J, et al. Proton MR spectroscopy improves discrimination between tumor and pseudotumoral lesion in solid brain masses. *AJNR Am J Neuroradiol*. 2009;30:544-551.
- **30.** Cordova JS, Shu H-KG, Liang Z, et al. Whole-brain spectroscopic MRI biomarkers identify infiltrating margins in glioblastoma patients. *Neuro Oncol.* 2016;18:1180-1189.

**TABLE 1.** Results depending on different model terms in the logistic regression analysis.<sup>†</sup>

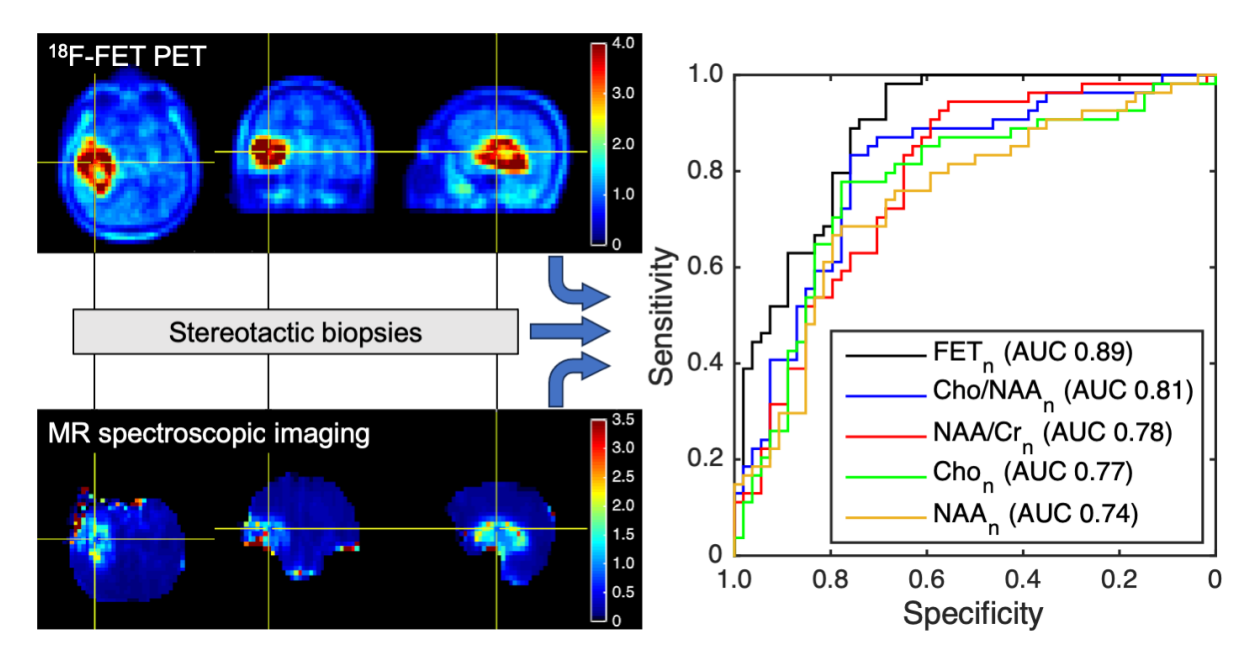
	AUC	Confidence		P intercept (l. 1)	
Marker	ROC	interval	Threshold	P slope (II. 2-4)	
FET <sub>n</sub> *	0.89	0.81 - 0.93	1.4	3.7e-06 3.4e-06	
Cho/NAA <sub>n</sub> *	0.81	0.71 - 0.88	2.16	5e-04 2e-04	
Cho/NAA *	0.79	0.68 - 0.86	0.65	0.0014 4.8e-04	
Cho/Cr <sub>n</sub> *	0.72	0.61 - 0.80	1.65	7.5e-04 6.9e-04	
Cho/Cr *	0.71	0.60 - 0.80	0.39	8.6e-04 8e-04	
NAA/Cr <sub>n</sub> *	0.78	0.68 - 0.86	0.76	4.8e-05 1.8e-05	
NAA/Cr *	0.75	0.65 - 0.84	0.86	1.1e-04 2.9e-05	
mIno/Cr <sub>n</sub> *	0.70	0.59 - 0.79	0.99	0.006 0.004	
Cho <sub>n</sub> *	0.77	0.67 - 0.85	1.37	0.001 0.001	
Cho *	0.71	0.60 - 0.80	10,594	0.037 0.024	
NAA <sub>n</sub> *	0.74	0.64 - 0.83	0.66	2.4e-04 9e-05	
NAA *	0.72	0.61 - 0.81	22,129	0.003 0.001	
mlno <sub>n</sub> *	0.70	0.59 - 0.79	0.87	0.01 0.01	
FET <sub>n</sub> , Cho/NAA <sub>n</sub>	0.90	0.82 - 0.94	n.a.	2.6e-06 6.2e-05 0.30539	
FET <sub>n</sub> , Cho/NAA	0.89	0.81 - 0.94	n.a.	2.4e-06 3.5e-05 0.56319	

 $<sup>^{\</sup>dagger}$  All models contain a constant and one or two linear terms, which represent the level of the markers O-(2-[18F]fluoroethyl)-L-tyrosine (FET), choline (Cho), N-acetyl-aspartate (NAA), creatine (Cr), myo-inositol (mIno), and ratios thereof. Signals normalized to normal-appearing tissue signal levels are denoted by the subscript "n". The table is limited to results where the normalized metabolite signal  $S_n$  reached an AUC of 0.70 or more. \*: p < 0.05 in all terms of the model.

**TABLE 2.** Results of the leave-one-out cross-validation

	<sup>18</sup> F-FET	Cho/NAA
Mean AUC ± SD	$0.89 \pm 0.003$	$0.81 \pm 0.004$
Mean Threshold ± SD	$1.4 \pm 0.01$	$2.16 \pm 0.04$
Accuracy	0.78	0.71
Sensitivity	0.76	0.59
Specificity	0.80	0.83
Positive predictive value	0.79	0.78
Negative predictive value	0.77	0.67

# **Graphical Abstract**



# Supplemental Data

#### **MR** Imaging

All studies were carried out on a Siemens (Erlangen, Germany) 3T TIM Trio with a Siemens 8-channel head coil. At the time of the <sup>18</sup>F-FET PET measurement, T1-weighted MRI data were acquired using an MPRAGE sequence (TR = 2.25 s, TE = 3.03 ms, in plane FOV 256 × 192, resolution 1 x 1 x 1 mm³, 256 sagittal slices acquired with zero gap) before and after the administration of a contrast agent (Gd-Dota, Dotarem™, Guerbet, 95943 Roissy, France). Moreover, MRI included a T2 (TR = 5.0 s, TE = 456 ms, in plane FOV 256 × 256, resolution 1 mm, 176 sagittal slices acquired with zero gap), and a FLAIR sequence (TR = 5.0 s, TE = 453 ms, in plane FOV 250 × 235, resolution 1 mm isotropic, 288 slices acquired with zero gap). A second contrast-enhanced T1-weighted MRI scan was acquired just before the stereotactic surgery, and a cranial computed tomography scan was conducted with the attached stereotactic frame for biopsy planning.

## MR Spectroscopic Imaging

The high-resolution whole-brain volumetric MRSI acquisition used a spin-echo excitation with echo-planar readout(1), TR = 1551 ms, TE =17.6 ms, FOV = 280 × 280 × 180 mm³ covering the cerebrum, 50[read] × 50[phase] × 18[slice] voxels, low flip angle excitation, and 1000 spectral sample points with a sweep width of 2500 Hz. It took 16 min of acquisition time. The integrated lipid suppression used an inversion recovery method with TI = 198 ms. The metabolite signals were acquired under chemical shift-selective water suppression and scaled with an unsuppressed water reference signal, which was gained from interleaved measurements with low flip angle and gradient-echo excitation.

#### **PET Imaging**

The synthesis procedure of <sup>18</sup>F-FET has been described previously.(2,3) All patients fasted for at least 12 hours prior to the PET measurement and were injected intravenously with 3 MBq/kg

body weight of <sup>18</sup>F-FET. The measurement was carried out with a Siemens BrainPET detector insert(*4*) integrated in the MR scanner. Dynamic data with an image resolution range between ~3 mm at the center and ~5 mm at 10 cm radial distance were acquired over 50 min and framed into 5×1 min, 5×3 min, and 6×5 min consecutive time periods during the reconstruction. The reconstruction matrix comprised 256 × 256 × 153 voxels with an isotropic voxel size of 1.25 mm. The image reconstruction comprised the correction steps for dead time, scatter, and random events, as well as for the attenuation correction based on an attenuation map template derived from PET data and registered to the T1 data set.(*5*)

All the reconstructed frames were smoothed with a 2.5 mm Gaussian kernel and motion corrected using PMOD (v3.5, Zürich, Switzerland). The summed images from 20 to 40 min post-injection were used for the analysis.

#### **Stereotactic Biopsies**

Before stereotactic biopsy, contrast-enhanced MRI and <sup>18</sup>F-FET PET were spatially registered on an intraoperatively obtained cranial CT as a basic image for planning the biopsy trajectory. The trajectory targeted the area with the highest <sup>18</sup>F-FET uptake while avoiding vessels and eloquent brain areas. During stereotactic biopsy, cylindrical specimens with a diameter of 2.8 mm and a length of 5-10 mm were taken along the trajectory, and their individual coordinates were stored. The samples, collected between July 2018 and September 2020, were evaluated by two experienced neuropathologists (M.D., A.B.) as part of routine diagnosis at the Institute of Neuropathology, University Hospital Cologne, and were (re)classified according to the 2021 World Health Organization (WHO) Classification of Tumors of the Central Nervous System (CNS) taxonomy.(18) For ethical reasons, samples could not be taken from healthy brain tissue; thus, the number of control samples was underrepresented. In order to balance the groups of samples for statistical analysis, "virtual negative biopsies" (i.e., the non-invasive examination of healthy-appearing contralateral brain regions using <sup>18</sup>F-FET PET and MRSI) were placed on the contralateral side with a margin of at least 4 cm around the tumor volume to minimize the risk of acquiring data from tissue that had already been microscopically

infiltrated.(6,7) Within this area, a sphere with a radius of 1.3 cm was positioned as close as possible to the site of the mirrored real biopsy. From this sphere, voxels with a maximum partial volume of white matter were selected. The number of chosen voxels was equal to the number of voxels of the corresponding real biopsy.

#### **Neuropathological methods**

Hematoxylin & eosin staining and immunohistochemistry were performed on 4-µm serial sections of formalin-fixed, paraffin-embedded tissue. In addition, the *MGMT* gene promotor methylation status and the *IDH1/IDH2* gene mutation status were determined by pyrosequencing. In the case of an *IDH1* mutation in exon 132 or an *IDH2* mutation in exon 172, respectively, the diagnostic algorithm was completed by microsatellite analysis to identify a 1p/19q codeletion and, thus, to differentiate between oligodendroglial and astrocytic tumors.

#### **Data Analysis**

The reconstruction of the spectroscopic data was carried out using the Metabolite Imaging and Data Analysis System (MIDAS) software package.(8) After the interpolation from 50 × 50 × 18 to 64 × 64 × 32 voxels (4.375 x 4.375 x 5.625 mm³), including spatial smoothing, the final spatial resolution of 108 mm³, with 1,024 spectral sample points over a sweep width of 2,500 Hz was obtained. The data were transformed into volumetric metabolite maps by using automatic spectral analysis and following signal normalization to the simultaneously acquired water reference signal.(9) The maps comprised the metabolite distributions of Cho, Cr, NAA, and myo-Inositol (mIno). For the final analysis, ratio maps of Cho/NAA, NAA/Cr, Cho/Cre, and mIno/Cr were calculated.

The <sup>18</sup>F-FET PET, MRSI, all other MRI data, and the biopsy track masks were registered to the T1 data. Masks of the tumor and the surrounding edema were manually delineated based on the FLAIR and T2 data as described elsewhere(*10*) and included as "other" tissue in the FSL-FAST segmentation of the brain tissue in addition to the tissue classes grey/white matter (GM/WM) and cerebrospinal fluid (CSF). Moreover, the "other" tissue masks were used to

keep the normalization to the water signal devoid of distortions caused by the edema of the tumor tissue.

The <sup>18</sup>F-FET and metabolite data were normalized to the respective background signals, which were given by the mean signal outside of the area delineated by the previously described tumor masks in voxels with a total content of white and grey matter greater than 50%. This procedure is referred to below as normalization to normal-appearing tissue. The <sup>18</sup>F-FET images were resampled to the resolution of the metabolite maps. To enable comparison with literature values, the usual normalized <sup>18</sup>F-FET accumulation, <sup>18</sup>F-FET<sub>n</sub>, and normalized as well as nonnormalized metabolite values were further analyzed.

The biopsy masks were down-sampled to match the spatial resolution of the spectroscopic data. Voxels with a biopsy partial volume of less than 50% or an underlying spectral linewidth outside the interval from 3 to 12 Hz were excluded from further analysis.

In general, the biopsies did not fall entirely within a voxel of the image matrix but rather crossed the boundary of adjacent voxels. Therefore, the <sup>18</sup>F-FET uptake values and the above-listed metabolite signals were averaged over the number of voxels per biopsy at the location given by the biopsy masks. The histological findings "glial tumor" and "infiltration zone" were labeled as tumor tissue in terms of PET/MRS imaging. Benign results and findings that were positive only on the microscopic scale, such as "proliferated brain tissue with tumor cells" were considered negative.

The threshold for neoplastic tissue based on different metabolite combinations and/or <sup>18</sup>F-FET uptake was determined by logistic regression. The first analysis included single terms representing <sup>18</sup>F-FET uptake and the metabolite ratios Cho/NAA, Cho/Cr, NAA/Cr, and mlno/Cr. The area under the curve (AUC) of the receiver operating characteristic (ROC) was used to analyze the accuracy of the various terms to separate tumor from normal tissue. The metabolites with the highest AUC values were included in the subsequent combined analysis.

The results from the terms offering the greatest value for clinical application were validated by leave-one-out cross-validation. All these analyses were performed by custom Matlab(R2015a) code.

# Results

**Table S1** shows the individual characteristics and neuropathological diagnoses according to the 2021 WHO CNS classification.

Table S1 Patient characteristics

#	Age	Sex	Diagnosis according to WHO 2021 5th edition	Number of	MRI contrast
	[y]			biopsies	enhancement
1	41	M	Astrocytoma, IDH1-mutant (CNS WHO grade 3)	4	Yes
2	40	M	Astrocytoma, IDH1-mutant (CNS WHO grade 3)	2	No
3	50	F	Glioblastoma, IDH-wildtype (CNS WHO grade 4)	7	Yes
4	57	M	Glioblastoma, IDH-wildtype (CNS WHO grad 4)	3	Yes
5	50	F	Glioblastoma, IDH-wildtype (CNS WHO grade 4)	4	No
6	82	F	Oligodendroglioma, IDH1-mutant, 1p/19q-codeletion (CNS WHO grade 3)	3	Yes
7	61	F	Glioblastoma, IDH-wildtype (CNS WHO grade 4)	2	No
8	27	F	Oligodendroglioma, IDH1-mutant, 1p/19q-codeletion (CNS WHO grade 2)	3	No
9	45	M	Oligodendroglioma, IDH1-mutant, 1p/19q-codeletion (CNS WHO grade 3)	3	No
10	58	M	Glioblastoma, IDH-wildtype (CNS WHO grade 4)	3	Yes
11	60	M	Oligodendroglioma, IDH1-mutant, 1p/19q-codeletion (CNS WHO grade 3)	1	No
12	60	M	Astrocytoma, IDH1-mutant (CNS WHO grade 4)	2	Yes
13	36	F	Astrocytoma, IDH1-mutant (CNS WHO grade 2)	1	No
14	58	M	Glioblastoma, IDH-wildtype (CNS WHO grade 4)	1	Yes
15	37	M	Astrocytoma, IDH1-mutant (CNS WHO grade 4)	4	Yes
16	34	F	CD4 T cell-dominated encephalitis	2	Yes
17	49	M	Oligodendroglioma, IDH1-mutant, 1p/19q-codeletion (CNS WHO grade 2)	3	No
18	66	F	Glioblastoma, IDH-wildtype (CNS WHO grade 4)	5	Yes
19	38	F	Oligodendroglioma, IDH1-mutant, 1p/19q-codeletion (CNS WHO grade 2)	3	No
20	37	F	Oligodendroglioma, IDH1-mutant, 1p/19q-codeletion (CNS WHO grade 2)	3	No
21	52	F	Brain tissue with reactive alterations	3	No
22	32	F	Oligodendroglioma, IDH1-mutant, 1p/19q-codeletion (CNS WHO grade 2)	4	No
23	42	F	Brain tissue with discrete increased cellularity	2	No
24	35	M	Astrocytoma, IDH1-mutant (CNS WHO grade 3)	4	No
25	28	M	Oligodendroglioma, IDH1-mutant, 1p/19q-codeletion (CNS WHO grade 2)	2	No
26	58	M	Brain tissue with reactive alterations	3	No
27	32	M	Astrocytoma, IDH1-mutant (CNS WHO grade 3)	3	No
28	62	F	Cerebral ischemia stage II/III	2	Yes
29	44	M	Brain tissue with discrete reactive alterations	4	No
30	62	M	Glioblastoma, IDH-wildtype (CNS WHO grade 4), TERT-promoter mutated	2	No

Four out of 35 patients were excluded from the analysis because of insufficient spectral quality. The corresponding <sup>18</sup>F-FET uptake values, expressed as the tumor-to-background ratio, are shown in Table S2.

**Table S**2 <sup>18</sup>F-FET uptake expressed as tumor-to-background ratio (TBR) of the four patients who were excluded due to insufficient MRSI quality. The number of <sup>18</sup>F-FET TBR values corresponds to the number of biopsies. MRI contrast enhancement (CE).

	Age	Sex	Diagnosis	MRI	<sup>18</sup> F-FET TBR
	[y]			CE	
1	46	F	Brain tissue with reactive alterations	No	1.57, 1.67
2	55	M	Glioblastoma, IDH-wildtype (CNS WHO grade 4)	Yes	3.04, 5.95, 2.97
3	54	М	Oligodendroglioma, IDH1-mutant, 1p/19q-codeletion (CNS WHO grade 2)	No	1.37
4	43	М	Glioblastoma, IDH-wildtype (CNS WHO grad 4)	Yes	1.67, 2.33

The additional introduction of the interaction term between <sup>18</sup>F-FET<sub>n</sub> uptake and Cho/NAA<sub>n</sub> resulted in a significant finding with an accuracy comparable to the <sup>18</sup>F-FET-only analysis (Table S3). Therefore, this more complicated model was excluded from subsequent analysis steps.

**Table S3** Results depending on the interaction term between <sup>18</sup>F-FET<sub>n</sub> and Cho/NAA<sub>n</sub> in the logistic regression analysis.

Model terms	AUC ROC	Confidence interval	Threshold	p intercept (l. 1) p slope (ll. 2-4)
Const, <sup>18</sup> F-FET <sub>n</sub> , Cho/NAA <sub>n</sub> , interaction(FET,Cho/NAA) *	0.90	0.82 - 0.94	n.a.	2.1e-06 1.1e-05 0.004 0.002
Const, <sup>18</sup> F-FET <sub>n</sub> , Cho/NAA, interaction(FET,Cho/NAA) *	0.89	0.82 - 0.94	n.a.	2.9e-06 1.3e-05 0.009

<sup>\*</sup> p < 0.05 in all terms of the model

#### **REFERENCES**

- **1.** Ebel A, Maudsley AA. Detection and correction of frequency instabilities for volumetric 1H echo-planar spectroscopic imaging. *Magn Reson Med.* 2005;53:465-469.
- 2. Hamacher K, Coenen HH. Efficient routine production of the 18F-labelled amino acid O-(2-[18F]fluoroethyl)-L-tyrosine. *Appl Radiat Isot.* 2002;57:853-856.
- **3.** Wester HJ, Herz M, Weber W, et al. Synthesis and radiopharmacology of O-(2-[18F]fluoroethyl)-L-tyrosine for tumor imaging. *J Nucl Med.* 1999;40:205-212.
- **4.** Herzog H, Langen K-J, Weirich C, et al. High resolution BrainPET combined with simultaneous MRI. *Nuklearmedizin*. 2011;50:74-82.
- 5. Rota Kops E, Hautzel H, Herzog H, Antoch G, Shah NJ. Comparison of Template-Based Versus CT-Based Attenuation Correction for Hybrid MR/PET Scanners. *IEEE Trans Nucl Sci.* 2015;62:2115-2121.
- **6.** Gates EDH, Lin JS, Weinberg JS, et al. Guiding the first biopsy in glioma patients using estimated Ki-67 maps derived from MRI: conventional versus advanced imaging. *Neuro Oncol.* 2019;21:527-536.
- **7.** Silbergeld DL, Chicoine MR. Isolation and characterization of human malignant glioma cells from histologically normal brain. *J Neurosurg.* 1997;86:525-531.

- **8.** Maudsley AA, Darkazanli A, Alger JR, et al. Comprehensive processing, display and analysis for in vivo MR spectroscopic imaging. *NMR Biomed*. 2006;19:492-503.
- **9.** Soher BJ, Young K, Govindaraju V, Maudsley AA. Automated spectral analysis III: application to in vivo proton MR spectroscopy and spectroscopic imaging. *Magn Reson Med.* 1998;40:822-831.
- **10.** Mauler J, Maudsley AA, Langen K-J, et al. Spatial Relationship of Glioma Volume Derived from <sup>18</sup>F-FET PET and Volumetric MR Spectroscopy Imaging: A Hybrid PET/MRI Study. *J Nucl Med.* 2018;59:603-609.